A three-dimensional high-order numerical model for the simulation of the interaction between waves and an emerged barrier

FRANCESCO GALLERANO, FEDERICA PALLESCHI, BENEDETTA IELE, GIOVANNI CANNATA
Department of Civil, Constructional and Environmental Engineering
Sapienza University of Rome
Via Eudossiana 18, 00184, Rome
ITALY

Abstract: - We present a new three-dimensional numerical model for the simulation of breaking waves. In the proposed model, the integral contravariant form of the Navier-Stokes equations is expressed in a curvilinear moving coordinate system and are integrated by a predictor-corrector method. In the predictor step of the method, the equations of motion are discretized by a shock-capturing scheme that is based on an original high-order scheme for the reconstruction of the point values of the conserved variables on the faces of the computational grid. On the cell faces, the updating of the point values of the conserved variables is carried out by an exact Riemann solver. The final flow velocity field is obtained by a corrector step which is based exclusively on conserved variables, without the need of calculating an intermediate field of primitive variables. The new three-dimensional model significantly reduces the kinetic energy numerical dissipation introduced by the scheme. The proposed model is validated against experimental tests of breaking waves and is applied to the three-dimensional simulation of the local vortices produced by the interaction between the wave motion and an emerged barrier.

Key-Words: - breaking waves, wave-structure interaction, vortices, high-order scheme, exact Riemann solver, three-dimensional simulation

Received: June 9, 2021. Revised: May 21, 2022. Accepted: June 19, 2022. Published: July 18, 2022.

1 Introduction

The three-dimensional numerical simulation of gravity wave motion can be carried out by numerically solving the Navier-Stokes Equations. In the numerical simulation of the Navier-Stokes Equations for free-surface flows, one of the most challenging problems is the calculation of the free surface elevation. In this context, some of the first numerical models proposed in the literature [1,2] are based on a technique called volume of fluid (VOF) method. The VOF method is used to simulate the motion of two fluids (air and water) by solving a momentum balance equation for the mixture of the two fluids on a fixed Cartesian grid. The volume fraction of the gaseous phase is calculated by its continuity equation, while the continuity equation of the liquid phase takes the form of the divergence of the velocity field equal to zero. In the computational cells occupied only by water, the volume fraction of the gaseous phase is zero, while the volume fraction of the liquid phase is equal to one. In the computational cells occupied only by air, the volume fraction of the gaseous phase is equal to one, while the volume fraction of the liquid phase is null. The free surface is located in the computational cells occupied by both air and water. The numerical solution of the continuity equation for the gaseous phase is used to calculate the volume fraction of the air and, thus, to calculate the position of the free surface. In the above method, the free surface is not sharply defined and its position does not coincide with the boundary of a computational cell. Consequently, by this method it is not straightforward to impose boundary conditions for the pressure and the kinematic boundary condition at the free surface [3]. Furthermore, the adoption of fixed Cartesian grids entails high computational costs that make the application of this method to real-scale numerical simulations of wave motion very expensive. A different kind of numerical models that are used to simulate free-surface flows is based on the Smoothed Particle Hydrodynamics (SPH) [4-6]. This approach can produce very accurate representations of the free-surface hydrodynamics but is usually limited to small-size flow problems because its high computational cost.
In an alternative class of numerical models for the three-dimensional simulation of free-surface flows,

the Navier-Stokes Equations are written in a system of coordinates where the horizontal ones are Cartesian, while the vertical one is a moving coordinate (called $\sigma - coordinate$) obtained by a time-dependent transformation [7-9]. The above-mentioned numerical models have good dispersive properties that allow simulating the propagation of non-breaking waves by computational grids with less than ten nodes in the vertical direction. In Rouvinskaia et al. 2018 [10], a numerical model based on this method is used to simulate the internal wave impact on the pillars of hydraulic engineering constructions. In Zhang et al. 2021 [11] the same approach is used in a three-dimensional model for tsunami generation on irregular bathymetry.

The generalization of such an approach to time-varying physical domains characterized by an irregular shape has been proposed by [12], in which a contravariant integral contravariant formulation of the Navier-Stokes is written in time-dependent curvilinear coordinates. In [13-15] the above-mentioned motion equations are numerically integrated by a second-order accurate Total Variation Diminishing (TVD) shock-capturing scheme commonly used in the literature [7,8], which adopts an approximate Harten, Lax and van Leer (HLL) Riemann solver. By using the above shock-capturing scheme, a breaking wave is represented as a discontinuity in the numerical solution. It is known that, close to the discontinuities, the second-order TVD scheme reverts to first-order locally and, thus, introduces significant numerical dissipation of kinetic energy in the numerical solution. Furthermore, the approximate Riemann solver assumes a simplified wave structure of the solution of the Riemann problem that can produce too dissipative solutions. As a consequence, the numerical simulations of breaking waves carried out by a second-order accurate TVD shock-capturing scheme and an approximate Riemann solver are affected by some errors: the increase in wave amplitude during the shoaling process and the maximum height of the waves are poorly predicted; the position of the wave-breaking point and the reduction of the wave height that take place after the wave breaking are not correctly simulated. The application of such low-order dissipative schemes for the numerical simulation of breaking waves and wave-induced currents requires very fine computational grids, which make them suitable mainly for simulations of laboratory-scale tests.

In this paper, we propose a new conservative non-hydrostatic shock-capturing numerical scheme for the numerical integration of the contravariant integral form of the Navier-Stokes equations proposed by [12]. The elements of novelty of the proposed numerical scheme are three. The state of the system is given by the field of the conserved variables, H and Hu^k, in which H is the total water depth and u^k are the contravariant component of the three-dimensional flow velocity. The first element of novelty is given by the fact that, in the proposed numerical scheme, the time-advancing of the numerical solution is carried out by a predictor-corrector procedure according to which an approximate field of the conserved variable $\left(Hu^k\right)_*$ is corrected by the gradient of a potential scalar function φ that take into account the non-hydrostatic pressure component. Differently from [12], in the present scheme, the scalar function φ is calculated by numerically integrating an equation of Poisson-type in which only the conserved variables $\left(Hu^k\right)_*$ are used, instead of the primitive variables $\left(u^k\right)_*$. By this strategy, in the presence of discontinuities, the proposed conservative scheme can converge to the correct weak solution. The second element of novelty concerns the reconstruction of the point values on the cell faces of the computational grid. In the proposed scheme, such point values are carried out by a high-order reconstruction procedure, based on an original Targeted Essentially Non-oscillatory scheme which is designed for the simulation of breaking waves. The third element of novelty consist on the proposal of an exact Riemann solver for updating the conserved variables on the cell faces. The abovementioned modifications significantly reduce the kinetic energy numerical dissipation introduced by the scheme. Consequently, the proposed numerical scheme differs from the ones present in the literature, because allows us to correctly represent the complex fully three-dimensional flow patterns, that take place around the coastal defence structures.

The proposed scheme is validated against experimental tests of breaking waves and is applied to the simulation of the vortices produced by the interaction between the wave motion and an emerged barrier. The hydrodynamic phenomena that occur due to this interaction can induce significant modifications in the coastal sediment transport and local scouring around the barriers.

2 The proposed numerical scheme

In the proposed numerical scheme, the equations of motion are obtained by the contravariant integral formulation of the mass conservation and momentum balance equations written in a time-dependent curvilinear coordinate system. The main

element of the mathematical procedure consists on the integration of the mass conservation and momentum balance equations in a moving control volume and the adoption of a time-dependent coordinate transformation by which the moving irregular control volume is converted in a fixed prismatic one. By omitting the mathematical details of the abovementioned procedure (that can be found in [12]), the resulting motion equations are

$$\frac{d}{dt}\int_{\Delta V_0}\left(\vec{\tilde{g}}^{(l)}\cdot\vec{g}_{(k)}Hu^k\sqrt{g_0}\right)d\xi^1d\xi^2d\xi^3+$$
$$\sum_{\alpha=1}^{3}\left\{\int_{\Delta A_0^{\alpha+}}\left(\vec{\tilde{g}}^{(l)}\cdot\vec{g}_{(k)}Hu^k(Hu^\alpha/H-v^\alpha)+\vec{\tilde{g}}^{(l)}\cdot\vec{g}^{(\alpha)}G\eta H\right)\sqrt{g_0}d\xi^\beta d\xi^\gamma\right.$$
$$\left.-\int_{\Delta A_0^{\alpha-}}\left(\vec{\tilde{g}}^{(l)}\cdot\vec{g}_{(k)}Hu^k(Hu^\alpha/H-v^\alpha)+\vec{\tilde{g}}^{(l)}\cdot\vec{g}^{(\alpha)}G\eta H\right)d\xi^\beta d\xi^\gamma\right\}=$$
$$-\int_{\Delta V_0}\left(\vec{\tilde{g}}^{(l)}\cdot\vec{g}^{(m)}\frac{\partial p}{\partial\xi^m}H\sqrt{g_0}\right)d\xi^1d\xi^2d\xi^3$$
$$+\sum_{\alpha=1}^{3}\left\{\int_{\Delta A_0^{\alpha+}}\left(\vec{\tilde{g}}^{(l)}\cdot\vec{g}_{(k)}\frac{R^{k\alpha}}{\rho}H\sqrt{g_0}\right)d\xi^\beta d\xi^\gamma-\int_{\Delta A_0^{\alpha-}}\left(\vec{\tilde{g}}^{(l)}\cdot\vec{g}_{(k)}\frac{R^{k\alpha}}{\rho}H\sqrt{g_0}\right)d\xi^\beta d\xi^\gamma\right\} \quad (1)$$

$$\frac{d}{dt}\int_{\Delta V_0}\left(H\sqrt{g_0}\right)d\xi^1d\xi^2d\xi^3$$
$$+\sum_{\alpha=1}^{3}\left\{\int_{\Delta A_0^{\alpha+}}\left((Hu^\alpha-Hv^\alpha)\sqrt{g_0}\right)d\xi^\beta d\xi^\gamma-\int_{\Delta A_0^{\alpha-}}\left((Hu^\alpha-Hv^\alpha)\sqrt{g_0}\right)d\xi^\beta d\xi^\gamma\right\}=0 \quad (2)$$

where H and Hu^k are the conserved variables, given by the water depth H and its product by the contravariant components of the flow velocity, u^k; $\eta=H-h$ is the free-surface elevation; h is the still water depth; G is the acceleration due to gravity; ρ is the water density; p is the dynamic pressure; $R^{k\alpha}$ are the contravariant components of the tensor of the stresses devoid of the pressure term. ξ^l is the $l-th$ curvilinear coordinate, which is expressed as a time-dependent function of the Cartesian coordinates, x^l, $\tau=t$, $\xi^1=\xi^1(x^1,x^2,x^3)$, $\xi^2=\xi^2(x^1,x^2,x^3)$,$\xi^3=\left(x^3+h(x^1,x^2)\right)/H(x^1,x^2,t)$. In such coordinate transformation, ξ^3 is a moving coordinate that changes over time according to the variations of the water depth and assumes values between 0 (at the bottom) and 1 (at the free surface). In Eq. (1) and (2), $\vec{g}^{(k)}=\partial\xi^k/\partial\vec{x}$ and $\vec{g}_{(k)}=\partial\vec{x}/\partial\xi^k$ are the contravariant and covariant base vectors, respectively; $H\sqrt{g_0}=H\vec{k}\cdot\left(\vec{g}_{(1)}\wedge\vec{g}_{(2)}\right)$ is the specific expression assumed by the coordinate transformation's Jacobian, which is obtained multiplying H by the scalar product between the vertical unit vector $\vec{k}$ and the first two covariant base vectors; ΔV_0 is the volume of a computational cell in the transformed space; $\Delta A_0^{\alpha+}$ and $\Delta A_0^{\alpha-}$ indicate, respectively, the area of the face of the computational cell on which coordinate ξ^α is constant that is placed at larger and lower values of ξ^α; v^α is the contravariant component of the velocity vector that express the movements of the generic coordinate ξ^α.

In this paper, Equations (1) and (2) are numerically integrated by an original predictor-corrector finite-volume scheme where the state of the system is defined by the conserved variables Hu^k. In the predictor step, a simplified form of Eq. (1), where the dynamic pressure is omitted, is discretized by a shock-capturing finite-volume scheme in which, at the faces of each computational cell, a couple of point values of each conserved variable is reconstructed by an original high-order targeted essentially non-oscillatory (TENO) procedure; these couples of point values of the conserved variables are assumed as initial values of the Riemann problem. In the present numerical scheme, the solution of each local Riemann problem is calculated by extending to the three-dimensional equations of motion the exact Riemann solver proposed by [16]. In this way, the complete structure of the wave solution is taken into account, removing the simplifications adopted by the approximate Riemann solvers proposed in [12-15]. The exact Riemann problem solution is used to calculate a predictor field of the conserved variables, $\left(Hu^k\right)_*$, that correspond to an approximated three-dimensional velocity field with non-zero divergence.

In the corrector step, by using exclusively the predictor field of the conserved variables, we define a Poisson equation which is written in the curvilinear coordinate system,

$$\frac{\partial\left(H\vec{g}^{(k)}\cdot\vec{g}^{(r)}\frac{\partial\varphi}{\partial r}\sqrt{g_0}\right)}{\partial\xi^k}=-\frac{\partial\left(Hu^k\right)_*\sqrt{g_0}}{\partial\xi^k} \quad (3)$$

in which the unknown variable is a scalar function φ. Eq. (3) is solved by a numerical iterative solver in which the convergence is accelerated by a

multigrid method. The final field of the conserved variables is obtained by adding the gradient of φ (multiplied by H) to the predictor field

$$Hu^k = H\vec{g}^{(k)} \cdot \vec{g}^{(r)} \frac{\partial \varphi}{\partial r} + \left(Hu^k\right)_* \quad (4)$$

After the correction of the field of the conserved variables, the position of the free surface is updated by numerically solving the continuity equation integrated over the vertical coordinate ξ^3, between 0 and 1.

The second element of novelty of the proposed numerical concerns the reconstruction procedure in the predictor step. Following the approach proposed by [17], we define a convex combination of three second-order interpolant polynomials, a function of the smoothness of the numerical solution and a dynamic threshold for choosing how many polynomials participate in the given reconstruction.

If all the three polynomials are used, the value of Hu^k on a given the cell face is calculated by a high order approximation that significantly limits the dissipation of kinetic energy due to the numerical scheme. If only one or two candidate interpolant polynomials participate to the reconstruction, Hu^k is calculated by a low order approximation that introduces numerical dissipation of kinetic energy and avoids spurious unphysical oscillations in the numerical solution. In the proposed procedure, differently from the existing TENO schemes [17], the value of this dynamic threshold depends on two factors: the smoothness of the numerical solution and the steepness of the front of the wave. During the numerical simulations, in the instants and in the grid nodes in which the front of the wave becomes so steep to be considered a breaking wave front, the dynamic threshold assumes its minimum values and, consequently, is reduced the tendency of the procedure to exclude one or two polynomials from the reconstruction. Thus, at the wave breaking fronts we obtain the maximum order of accuracy of the reconstructions and minimize the dissipation of kinetic energy introduced in the numerical solution by the numerical scheme. By this strategy, we entrust mainly to the turbulence model the task of representing the wave breaking energy dissipation and we leave mainly to the numerical scheme the task of avoiding the unphysical oscillations at the tail of the wave and at non-breaking fronts (where the turbulence model is less effective). Below, we describe the main mathematical aspects of the proposed procedure.

The point value of a given conserved variable on a face of the computational cell, $\left(Hu^k\right)_F$, is calculated by a convex combination of interpolant polynomials of second order, f_p (with $p = -1,0,1$),

$$\left(Hu^k\right)_F = \omega_{-1} f_{-1} + \omega_0 f_0 + \omega_1 f_1 \quad (5)$$

where ω_p are the so-called nonlinear weights of the combination, which are defined as

$$\omega_p = \frac{\delta_p \mathrm{L}_p}{\sum_{p=-1}^{1} \delta_p \mathrm{L}_p} \quad (6)$$

In Eq. (6), δ_p are coefficients that can be 0 or 1 and are used to exclude or not polynomials f_p from the combination; L_p are the linear weights and are calculated to obtain fifth-order accuracy if no polynomial is excluded from the combination. We indicate by χ_p (with $p = -1,0,1$) a normalized function that provides a measure of the smoothness of the second-order polynomial f_p and indicate by C_T a dynamic threshold value for χ_p. At every instant of the numerical simulation, χ_p are compared with C_T, in order to assign 0 or 1 to coefficient δ_p of Eq. (6),

$$\begin{aligned} &\delta_p = 0, \text{if } \chi_p < C_T \\ &\delta_p = 1, \text{if } \chi_p > C_T \end{aligned} \quad (7)$$

The values of the dynamic threshold C_T are given by

$$C_T = 10^{-n} \quad (8)$$

where exponent n depends on two fixed parameters, A_m and A_M, and two functions θ and θ_2

$$n = A_m + (\theta + \theta_2)(A_M - A_m) \quad (9)$$

In Eq. (9), A_m and A_M are, respectively, the assigned minimum and maximum for exponent n; functions θ and θ_2 can range between 0 and 1, and their sum can be at most 1. Function θ depends on the smoothness of the numerical solution [17]. θ_2 is an original function that we express as a function of the wave front steepness

$$\begin{aligned} &\theta_2 = \left(\frac{\partial \eta}{\partial t}\right) / \left(\frac{\partial \eta^*}{\partial t}\right) - 1, \text{if } \frac{\partial \eta}{\partial t} > \frac{\partial \eta^*}{\partial t} \\ &\theta_2 = 0, \text{if } \frac{\partial \eta}{\partial t} < \frac{\partial \eta^*}{\partial t} \end{aligned} \quad (10)$$

where $\partial\eta/\partial t$ is the rate of change of the free-surface elevation and $\partial\eta^*/\partial t$ is a threshold value behind which the wave is considered as a breaking

wave. By Eq. (10), function θ_2 is different from 0 only at the front of a breaking wave and increases as the steepness of the wave front increases. The proposed original reconstruction ensures high-order of accuracy at the front of the breaking waves, where kinetic energy dissipation is mainly demanded to the turbulence model. At the wave tails and non-breaking fronts (where θ_2 is null), exponent n depends only on θ, that is a function of the smoothness of the numerical solution. In these regions, where the turbulence model is less effective, the ability of the proposed numerical scheme to reduce the spurious (unphysical) oscillations is maximum.
Unlike the second-order TVD reconstructions adopted by [12-15], the proposed numerical scheme ensures good non-oscillatory properties, without introducing excessive numerical dissipation in the numerical solution.

3 Results

Emerged barriers are commonly used in coastal engineering. The interaction between the incoming waves and an emerged barrier can produce velocity and pressure fluctuations and very complex instantaneous three-dimensional flow patterns characterized by quasi-periodic vortices. These vortices usually occur downstream of the edge of the barrier and can produce the resuspension of solid particles from the sea bottom and local scour phenomena. In this section we apply the proposed model to the simulation of the quasi-periodic vortex formations that take place downstream of a vertical barrier that interacts with breaking waves. A rectangular $15\,m \times 3\,m$ coastal area is discretized by a computational grid shown in Fig.1, where incoming cnoidal waves are produced at x = 0, propagate from left to right on a 1:35 bottom slope, and interacts with a $2\,m$ long and $0.5\,m$ wide emerged barrier that is placed at $x = 7.1\,m$ (red line in Fig. 1). In both the x and y directions, the size of the computational cells ranges between $0.025\,m$ and $0.05\,m$; in the z-direction the water depth is discretized by 9 moving layers. During the simulation, the first calculation node is placed at an average distance from the bottom equal to $z^+ = 30$ (where $z^+ = zu^*/\nu$ is a dimensionless distance calculated by the friction velocity u^* and the water viscosity ν). The remaining grid nodes in the vertical direction are uniformly distributed along the water column. The boundary on which $y = 1\,m$ is treated as a reflecting boundary, on which the normal velocity component is assumed equal to zero, while a zero normal derivative is assumed for the remaining quantities. The opposite boundary ($y = 4\,m$) is treated as an open boundary, on which the normal derivative of every quantity is assumed equal to zero. As input boundary conditions we impose $0.125\,m$ high cnoidal waves, whose wave period is equal to $2\,s$. The eddy viscosity is expressed by a Smagorinsky turbulence model in which the Samgorinsky coefficient C_s ranges between 0.05 and 0.2. On the left boundary, at x = 0 m, a cnoidal wave with period T = 2 s and wave height H = 0.125 m is imposed. Such a wave is equal to the one experimentally reproduced by [18] on a channel with the same initial water depth and 1:35 sloping beach (without the emerged barrier). In Fig. 2 we show the comparison between the experimental result of [18] and the numerical results obtained by the proposed model. The wave height obtained with the numerical model is in very good agreement with the experimental results, as shown in Fig. 2. The breaking point is located around $x = 6.5\,m$ as the one obtained by experimental measurements. In order to quantify the agreement between the numerical and the experimental results, we compare the free-surface elevation by using the mean absolute percentage error (MAPE) [19]

$$MAPE = \frac{\sum_{i=1}^{n} \frac{|Rexp_i - Rnum_i|}{Rexp_i}}{n} \times 100 \qquad (11)$$

where $Rexp_i$ and $Rnum_i$ are respectively the experimental and numerical measurements.

MAPE	4.85%

Table 1 Mean absolute percentage error for the free-surface elevation.

The very low relative error between the proposed model and the experimental results (less than 5 per cent) demonstrates that the proposed model is able to correctly simulate the wave shoaling, the maximum wave height, the wave breaking point and the wave height reduction in the surf zone.

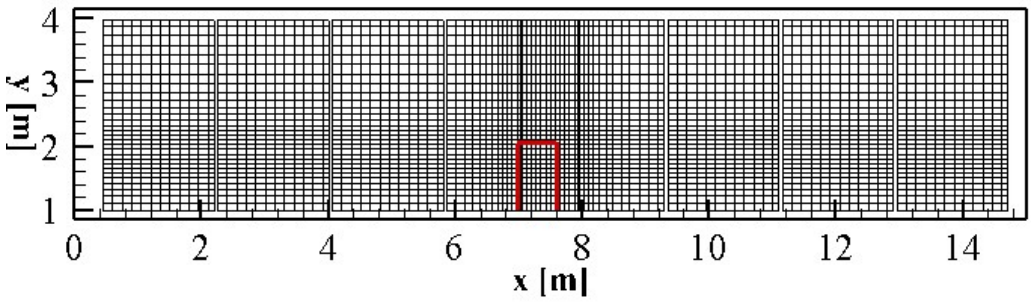

Fig.1. Computational grid (one grid line out of every three is drawn). The red line indicates the position of the emerged barrier.

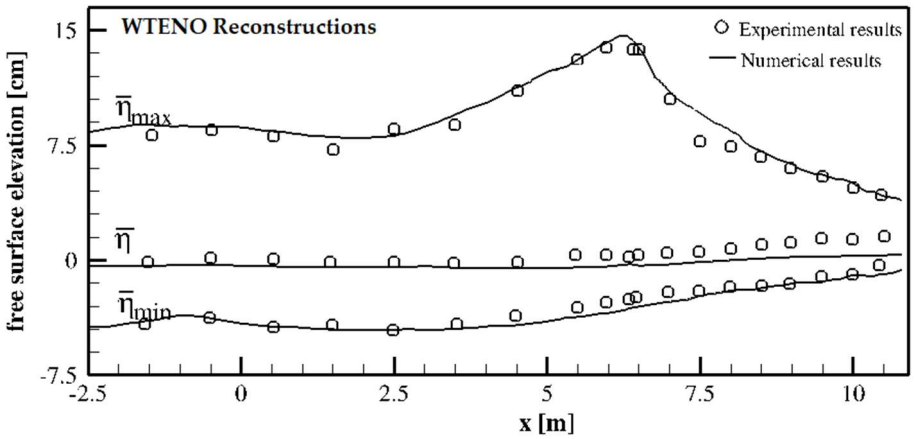

Fig. 2. Breaking wave. Maximum free-surface elevation, mean water level and minimum free-surface elevation. Circles: experimental measurements by [18]; lines: proposed model numerical results.

Fig. 3 shows three instants of the simulated free-surface elevation given by the interaction between the cnoidal waves and the emerged barrier. In such figures, the emerged barrier is not drawn and its basis is represented by the blue color. From Figs. 3(a) - 3(c) it is possible to see the wave height reduction produced by the breaking of the waves that approach the barrier and the reflection caused by the wave collision with the barrier. The spatial variations of the wave height caused by the interaction with the barrier produce currents which can be highlighted by averaging over time the instantaneous flow velocity components.

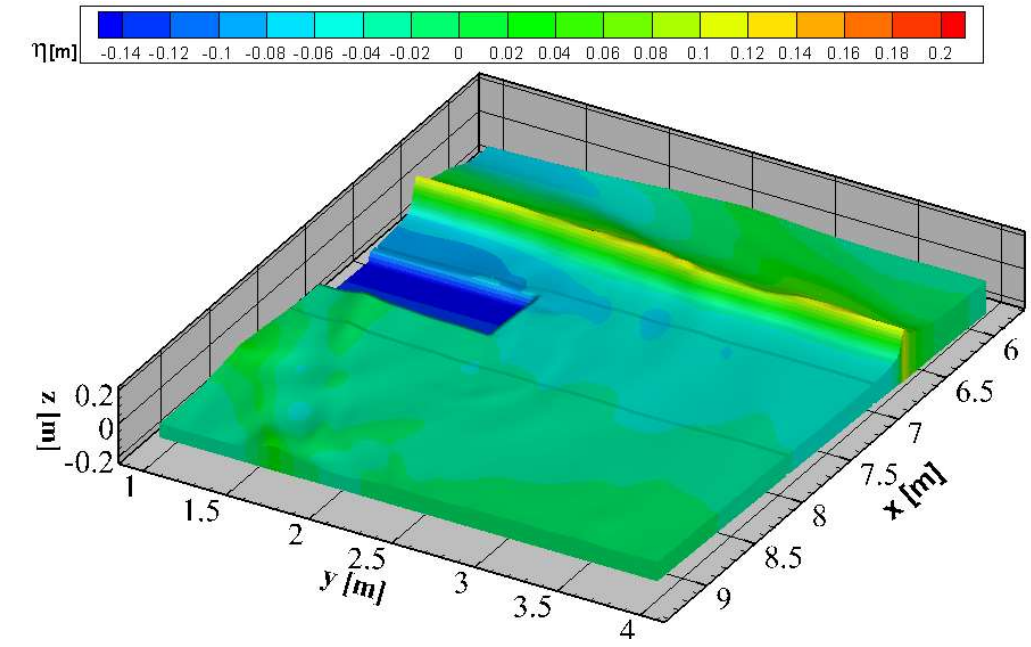
η [m]
-0.14 -0.12 -0.1 -0.08 -0.06 -0.04 -0.02 0 0.02 0.04 0.06 0.08 0.1 0.12 0.14 0.16 0.18 0.2
z [m]
0.2
0
-0.2
1
1.5
2
2.5
3
3.5
4
y [m]
6
6.5
7
7.5
8
8.5
9
x [m]

(a)

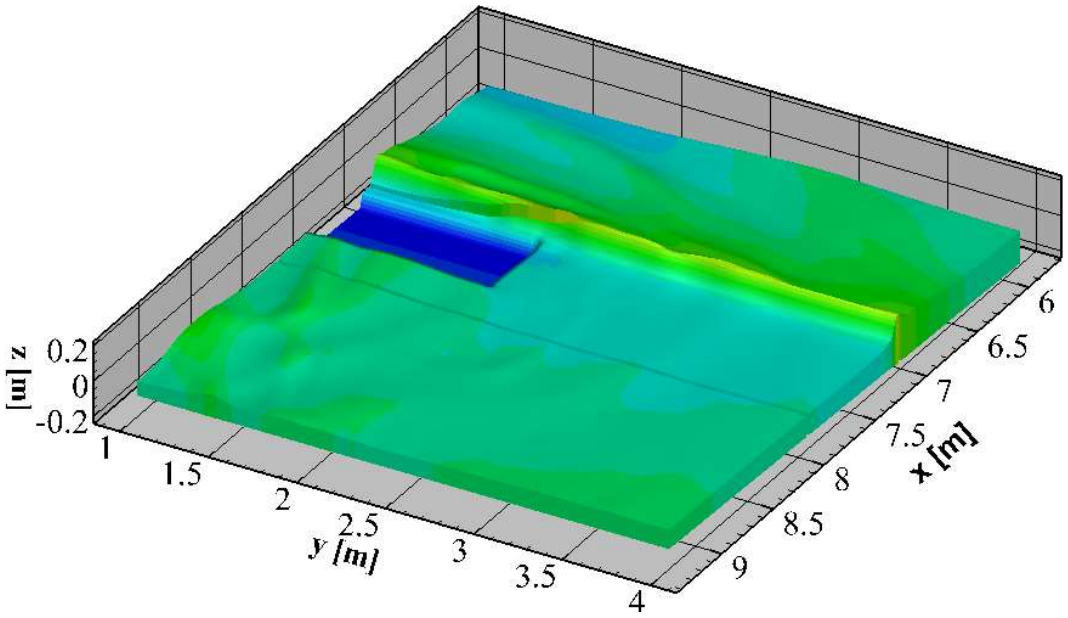
z [m]
0.2
0
-0.2
1
1.5
2
2.5
3
3.5
4
y [m]
6
6.5
7
7.5
8
8.5
9
x [m]

(b)

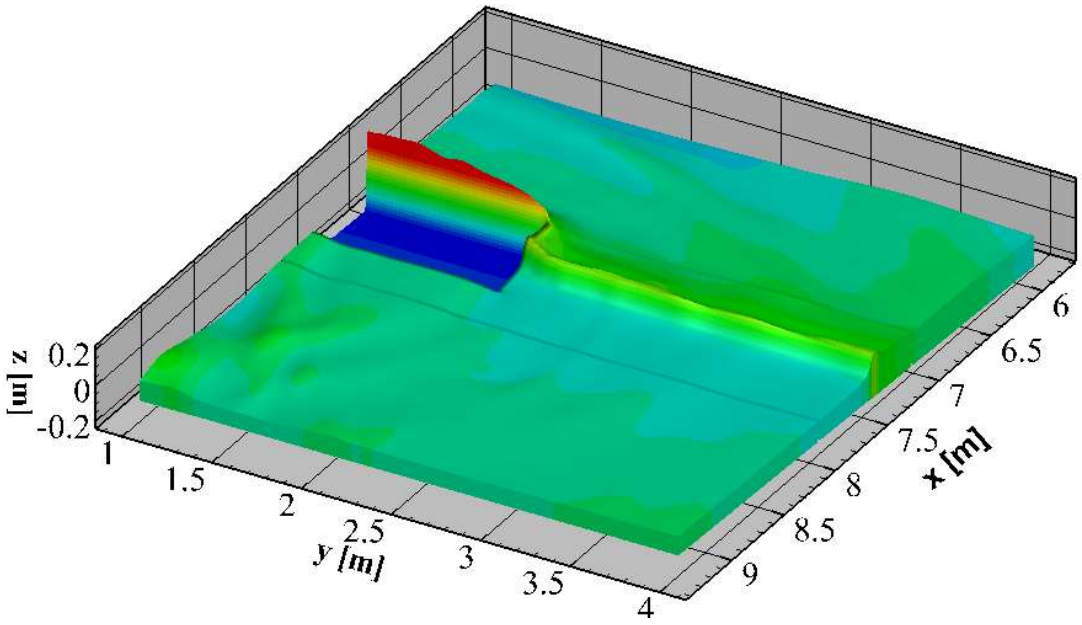

(c)

Fig. 3(a)-(c). A sequence of three instantaneous views of the simulated wave field

Fig. 4 shows the numerical results of the currents induced by the wave-structure interaction at three different depths: a) close to the seabed; b) at middle depth; c) close to the water surface. Fig. 4 shows that the interaction between the incoming waves and the barrier produces, at the onshore side of the barrier, a large eddy which turns in a clockwise sense and increases its intensity as the distance from the bottom increases.

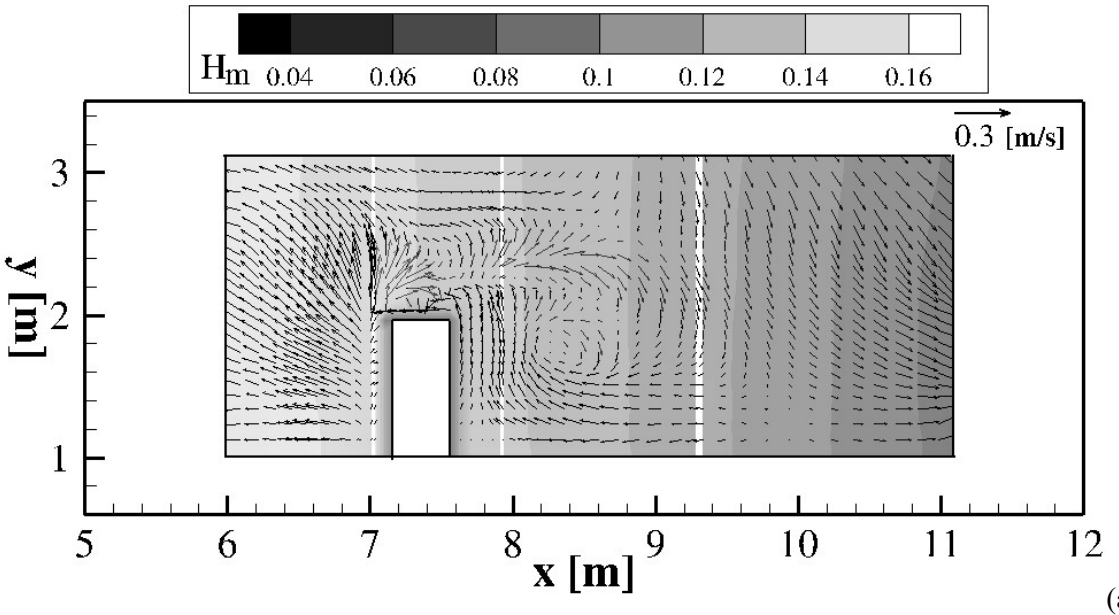

(a)

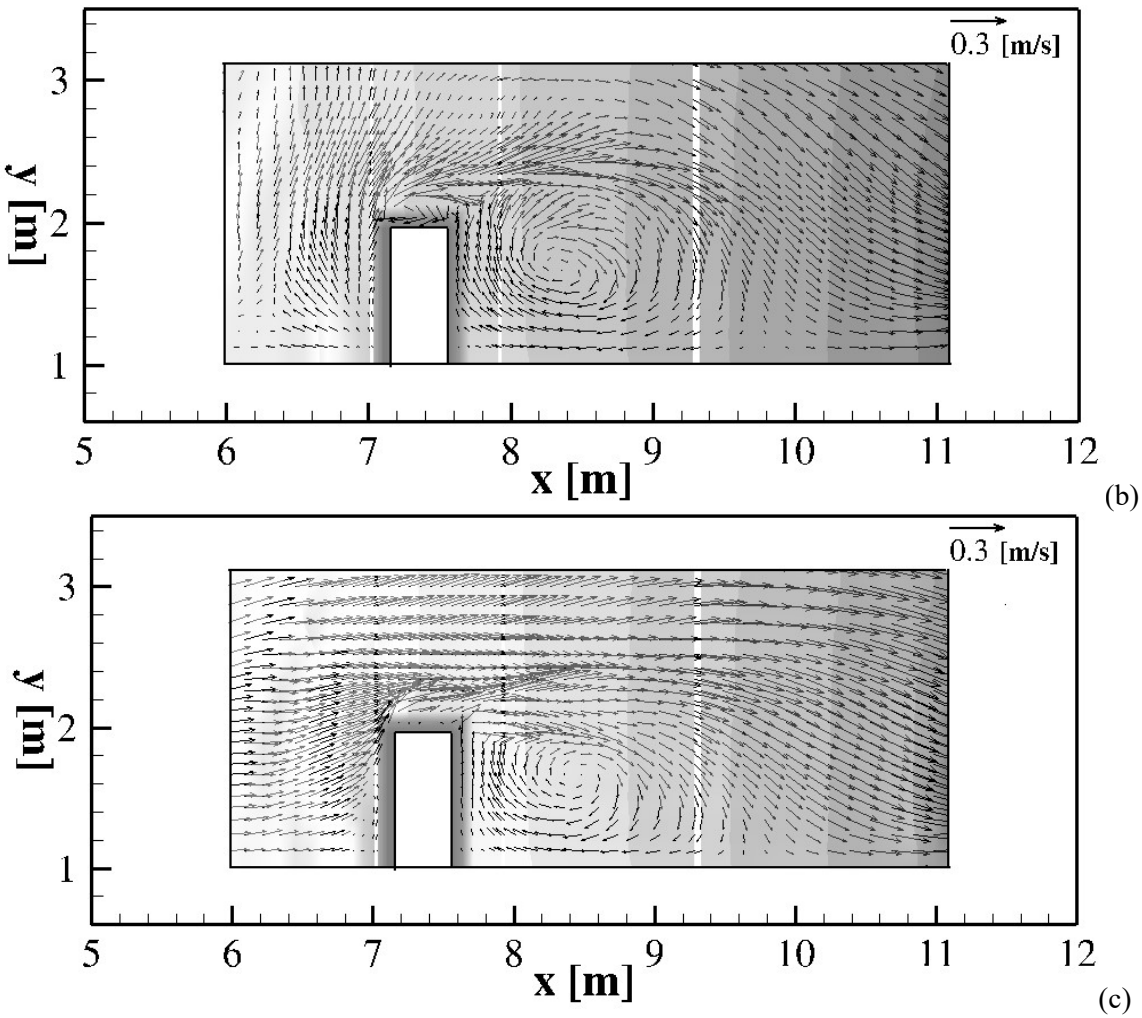

Fig. 4. Plan view of the simulated circulation patterns: (a) close to the seabed; (b) at middle depth; (c) close to the water surface.

In Fig. 5 the quasi periodic vortices that take place near the barrier and propagate in the direction of the waves are visualized by the so-called Q-method for the vortices identification [20], according to which positive values of the second invariant of the velocity gradient tensor (denoted by Q) indicate the presence of a vortex. Fig. 5 shows that vortices characterized by a vertical axis take place close the barrier edges, starting from the seabed; as the distance from the barrier edges increases, the orientation of these vortices changes and tends to the direction of the propagation of the waves. These vortex structures can put into suspension the solid particles from the seabed and produce local erosion phenomena near the barrier.

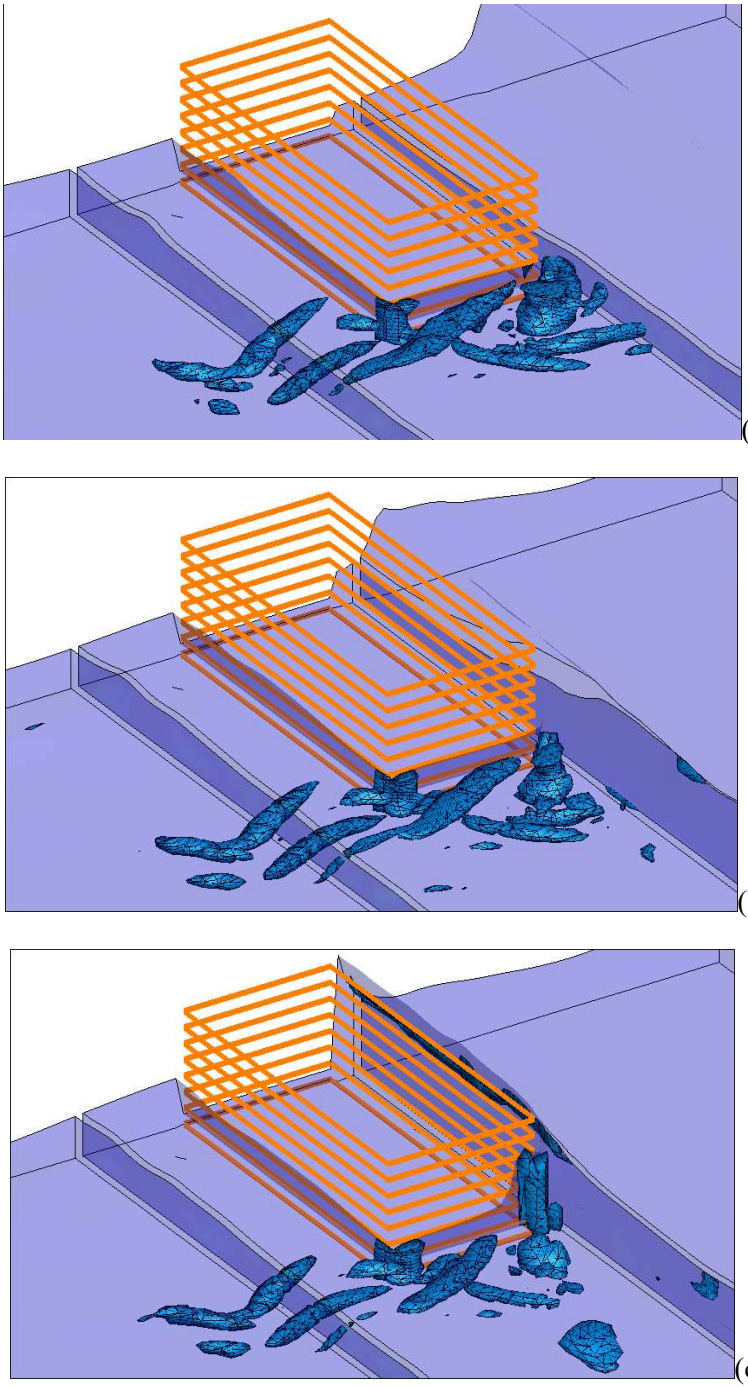

Fig. 5. Vortex structures identified by the Q-method ($Q = 3.5$).

4 Discussion

The proposed numerical model differs from the ones present in the literature; this model significantly reduces the kinetic energy numerical dissipation introduced by the scheme and allows us to correctly represent the complex fully three-dimensional flow patterns, that take place around the coastal defence structures. By the simulation of the vortices produced by the interaction between the wave motion and an emerged barrier, it can be notice that the proposed numerical model correctly represents the hydrodynamic phenomena that can induce significant modifications in the coastal sediment transport and local scouring around the barriers.

5 Conclusion

A numerical model for the three-dimensional numerical simulation of wave-structure interactions has been presented. The equations of motion at the

basis of the numerical model are expressed in a moving coordinate system and are integrated by an original conservative shock-capturing numerical scheme. The main element of originality of the proposed numerical scheme is given by an original TENO scheme specifically designed to simulate the breaking of the waves; the local Riemann problem produced by the TENO reconstruction procedure is solved by an exact Riemann solver. By the proposed numerical scheme, the three-dimensional flow structures produced by the interaction between trains of breaking waves and a coastal defence structure parallel to shoreline has been simulated. The results obtained by the proposed numerical scheme show that by this approach it is possible to represent both the large scale hydrodynamic phenomena, like the wave-induced circulation patterns downstream the barrier, and small scale flow structures, like the quasi periodic vortices that take place near the barrier's edges, close to the bottom. Both the hydrodynamic phenomena are fully three-dimensional and can induce significant modifications in the coastal sediment transport and local scouring around the barriers.

References:

[1] Bradford S.F., Numerical simulation of surf zone dynamics, *Journal of Waterway, Port, Coastal, and Ocean Engineering,* 126, 1, 2000, pp. 1-13.

[2] Higuera P, Lara J.L., Losada I.J., Simulating coastal engineering processes with OpenFOAM®, *Coastal Engineering*, 71, 2013, pp. 119-134.

[3] Lin P., Li C.W., A σ-coordinate three-dimensional numerical model for surface wave propagation, *International Journal for Numerical Methods in Fluids,* 38, 11, 2002, pp. 1045-1068.

[4] Price D.J., Smoothed particle hydrodynamics and magnetohydrodynamics, *Journal of Computational Physics*, 231(3), 2012, pp. 759–794.

[5] Yang X., Peng S., Liu M., A new kernel function for sph with applications to free surface flows, *Applied Mathematical Modelling*, 38(15-16), 2014, pp. 3822–3833.

[6] Perea J., Cordero J., A Stable Hybrid Potential–SPH Technique to Enforce the Fluid Incompressibility, *WSEAS Transactions on Fluid Mechanics*, 13, 2018, pp. 50-59.

[7] Bradford S.F., Nonhydrostatic model for surf zone simulation, *Journal of Waterway, Port, Coastal, and Ocean Engineering*, 137, 4, 2011, pp. 163-174.

[8] Ma G., Shi F., Kirby J., Shock-capturing non-hydrostatic model for fully dispersive surface wave processes, *Ocean Modelling*, 43, 2012, pp. 22-35.

[9] Iele B., Palleschi F., Gallerano F., Boundary conditions for the simulation of wave breaking, *WSEAS Transaction on Fluid Mechanics*, 15, 2020, pp.41-53.

[10] Rouvinskaia E., Kurkina O., Kurkin A., Zaytsev A., Modeling of internal wave impact on hypothetical pillars of hydraulic engineering constructions in the conditions of the Sakhalin island shelf, *WSEAS Transactions on Fluid Mechanics*, 13, 2018, pp. 101-107.

[11] Zhang C., Kirby J.T., Shi F., Ma G., Grilli, S.T., A two-layer non-hydrostatic landslide model for tsunami generation on irregular bathymetry. 2. Numerical discretization and model validation, *Ocean Modelling*, 160, 2021, pp. 101769.

[12] Cannata G., Petrelli C., Barsi L., Gallerano F., Numerical integration of the contravariant integral form of the Navier–Stokes equations in time-dependent curvilinear coordinate systems for three-dimensional free surface flows, *Continuum Mechanics and Thermodynamics*, 31, 2, 2019, pp. 491-519.

[13] Tamburrino M., Cannata G., Simulation of wave run-up by means of the exact solution of the wet/dry Riemann problem, *WSEAS Transactions on Fluid Mechanics*, 14, 2019, pp. 114-123.

[14] Gallerano F., Cannata G., Tamburrino M., Ferrari S., Badas M.G., Querzoli G., Water waves overtopping over barriers, *WSEAS Transactions on Fluid Mechanics*, 14, 2019, pp. 84-91.

[15] Gallerano F., Cannata G., Barsi L., Palleschi, F., Iele B. Simulation of wave motion and wave breaking induced energy dissipation, *WSEAS Transactions on Fluid Mechanics*, 14, 2019, pp. 62-69.

[16] Toro E.F., *Shock-capturing methods for free-surface shallow flows*, Wiley-Blackwell, 2001.

[17] Peng J., Liu S., Li S., Zhang K., Shen Y., An efficient targeted ENO scheme with local adaptive dissipation for compressible flow simulation, *Journal of Computational Physics*, 425, pp. 109902.

[18] Ting F.C.K., Kirby J.T., Observation of undertow and turbulence in a wave period, *Coastal Engineering,* 24, 1994, pp. 51-80.

[19] Hyndman R. J., Koehler A. B. Another look at measures of forecast accuracy, *International Journal of forecasting*, 22, 2006, pp. 679-688.

[20] Hunt J.C., Wray A.A., Moin P., Eddies, streams, and convergence zones in turbulent flows, *Studying turbulence using numerical simulation databases, 2. Proceedings of the 1988 summer program,* 1988, pp. 193-208.

Contribution of individual authors to the creation of a scientific article (ghostwriting policy)

Francesco Gallerano and Giovanni Cannata conceptualized the model and ideated the scheme. Federica Palleschi and Benedetta Iele carried out the validation and application of the proposed model.

Sources of funding for research presented in a scientific article or scientific article itself

This research received no external funding.